

Multiplex spatial analysis reveals increased CD137 expression and m-MDSC neighboring tumor cells in refractory classical Hodgkin Lymphoma

José L. Solórzano^{a,b*}, Victoria Menéndez^{b*}, Edwin Parra^c, Luisa Solís^c, Ruth Salazar^d, Mónica García-Cosío^e, Fina Climent^f, Sara Fernández^a, Eva Díaz^b, Alejandro Francisco-Cruz^g, Joseph Khoury^h, Mei Jiang^c, Auriole Tamegnon^c, Carlos Montalbán^b, Ignacio Meleroⁱ, Ignacio Wistuba^c, Carlos De Andreaⁱ, and Juan F. García^{a,b}

^aPathology and Molecular Department, MD Anderson Cancer Center, Madrid, Spain; ^bTranslational Research Department, MD Anderson Foundation, Madrid, Madrid, Spain; ^cDepartment of Translational Molecular Pathology, MD Anderson Cancer Center, Houston, Houston, TX, USA; ^dSan Agustín National University, Arequipa, Peru; ^ePathology Department, Hospital Ramón y Cajal, Madrid, Spain; ^fPathology Department, Hospital Universitari de Bellvitge, IDIBELL, L'Hospitalet De Llobregat, Barcelona, Spain; ^gPathology Department, National Institute of Cardiology Ignacio Chavez, México DF, Mexico; ^hDepartment of Pathology and Microbiology, University of Nebraska Medical Center, Omaha, NE, USA; ⁱUniversity of Navarra and Instituto de Investigación Sanitaria de Navarra, Pamplona, Navarra, Spain

ABSTRACT

The Hodgkin and Reed – Sternberg (HRS) cells in classical Hodgkin Lymphoma (cHL) actively modify the immune tumor microenvironment (TME) attracting immunosuppressive cells and expressing inhibitory molecules. A high frequency of myeloid cells in the TME is correlated with an unfavorable prognosis, but more specific and rare cell populations lack precise markers. Myeloid-derived suppressor cells (MDSCs) have been identified in the peripheral blood of cHL patients, where they appear to be correlated with disease aggressiveness. TNFRSF9 (CD137) is a T cell co-stimulator expressed by monocytic and dendritic cells. Its expression has also been described in HRS cells, where it is thought to play a role in reducing antitumor responses. Here, we perform qualitative and quantitative analyses of lymphocytic and MDSC subtypes and determine the CD137 cell distribution in cHL primary tumors using multiplex immunofluorescence and automated multispectral imaging. The results were correlated with patients' clinical features. Cells were stained with specific panels of immune checkpoint markers (PD-1, PD-L1, CD137), tumor-infiltrating T lymphocytes (CD3, PD-1), and monocytic cells/MDSCs (CD68, CD14, CD33, Arg-1, CD11b). This approach allowed us to identify distinct phenotypes and to analyze spatial interactions between immune subpopulations and tumor cells. The results confirm CD137 expression by T, monocytic and HRS cells. In addition, the expression of CD137, T exhausted cells, and monocytic MDSCs (m-MDSCs) in the vicinity of malignant HRS cells were associated with a worse prognosis. Our findings reveal new elements of the TME that mediate immune escape, and confirm CD137 as a candidate target for immunotherapy in cHL.

KEY POINTS

- CD137-expressing immune cells and HRS cells are more abundant and in closer proximity in refractory patients than in responders.
- Monocytic myeloid-derived suppressor cells (m-MDSCs) are associated with unfavorable outcomes and relapse in cHL, unlike granulocytic MDSCs (g-MDSCs), which are located far from HRS cells in non-responders.
- The cHL tumor microenvironment promotes immune escape in refractory patients by holistically driving polarization and/or recruitment of several cell types with increased expression of CD137 and PD-L1 checkpoints.

ARTICLE HISTORY

Received 14 May 2024
Revised 30 July 2024
Accepted 31 July 2024

KEYWORDS

Classical Hodgkin lymphoma; multiplex immunofluorescence; myeloid-derived suppressor cells (MDSCs); tumor microenvironment; tumor necrosis factor receptor 9 (TNFRSF9/CD137)

Introduction


The immune tumor microenvironment (TME) of classical Hodgkin lymphoma (cHL) tumors is a complex and heterogeneous milieu of ineffective immune cells and scattered neoplastic Hodgkin and Reed – Sternberg (HRS) cells.¹ The TME has been demonstrated to be induced and shaped by the HRS cells,² and plays a key role in the prognosis of the disease.

Cellular components of the TME include T and B cells, tumor-associated macrophages (TAMs), mast cells, eosinophils, myeloid-derived suppressor cells (MDSCs), cytotoxic

T and NK cells, plasma cells, and also stromal elements and blood vessels. Many of these cells can also secrete cytokines and chemokines that participate in the pathogenesis of the disease and are known to be associated with clinical outcome. Although most of the previous work has focused on studying the abundance of T cells and macrophages (mostly described as M2-like macrophages), an immunosuppressive response may also be attributed to some more infrequent but important immune cell phenotypes, as is the case of MDSCs.³

CONTACT Juan F. García  jfgarcia@mdanderson.es  Pathology Department, MD Anderson Cancer Center, C/Arturo Soria, 270, Madrid 28033, Spain

*These authors contributed equally to this work.

 Supplemental data for this article can be accessed online at <https://doi.org/10.1080/2162402X.2024.2388304>

© 2024 The Author(s). Published with license by Taylor & Francis Group, LLC.

This is an Open Access article distributed under the terms of the Creative Commons Attribution-NonCommercial License (<http://creativecommons.org/licenses/by-nc/4.0/>), which permits unrestricted non-commercial use, distribution, and reproduction in any medium, provided the original work is properly cited. The terms on which this article has been published allow the posting of the Accepted Manuscript in a repository by the author(s) or with their consent.

High frequencies of MDSCs are associated with poor prognosis and tumor progression in lymphomas.⁴ MDSCs have also been identified in the peripheral blood of cHL patients, where they seem to be associated with disease aggressiveness and to be prognostically significant.⁵ These cells are described by flow cytometry as lineages that co-express CD11b and CD33 molecules but lack HLA-DR,⁶ in contrast to normal monocytes and macrophages, and with an additional division into monocytic (m-MDSCs) and granulocytic (g-MDSCs) subsets. Depending on the source, m-MDSCs are defined as CD14+, or CD14low, while g-MDSCs are identified as CD14- or CD15+.

M-MDSCs are an important subset of MDSCs in B-cell lymphomas that block the immune responses.⁷ In fact, CD14+ m-MDSCs are correlated with a more aggressive disease, suppressed adaptive immunity, and a greater propensity to relapse post-therapy in non-Hodgkin lymphomas.⁸ On the other hand, g-MDSCs are considered low-density, and actively immunosuppressive.³ Some studies of g-MDSCs in cHL describing them as a CD14- population in peripheral blood have identified correlations with unfavorable prognosis.⁹

In addition, tumors can use immunological checkpoints as a protection against immune system attacks. The overexpression of PD-1 ligands by HRS cells is due to frequent copy gains of the 9p24.1 locus, which includes the PD-L1, PD-L2, and JAK2 genes.^{10,11} Clinical development concerning immunotherapy options has changed the therapeutic paradigm in cHL. That is the case of blocking the PD-1/PD-L1 axis, which can improve the progression-free survival (PFS) of 86% of patients with relapsed or refractory cHL.¹² However, the response to immunotherapy is neither completely effective nor durable in many patients, triggering the need to identify new, reliable biomarkers in the TME that could be targetable.

A newly described mechanism by which HRS cells can evade the immune system is the expression of the tumor necrosis factor receptor 9 (TNFRSF9, CD137, 4-1BB), a costimulatory glycoprotein receptor that is part of the tumor necrosis factor superfamily.¹³ CD137 acts as a T cell co-stimulator, expressed not only by T cells, monocytic and dendritic cells, but also by HRS cells. CD137 induces tumor cells to secrete IL-13, a potent growth factor that also polarizes the protective type 1 immune response toward a tumor-supporting type 2 response.¹⁴ It has been postulated that CD137 can be transferred from the HRS cells by trogocytosis to CD137 ligand (CD137L)-expressing antigen-presenting cells, leading to the formation of a CD137-CD137L complex and the internalization and degradation of CD137L.¹⁵ Since the CD137-CD137L interaction is a major driver of type I cellular immune responses, the elimination of CD137L might weaken the anti-tumor T cell response.

Until recently, studying the complex crosstalk between HRS cells and the surrounding TME was challenging. Conventional immunohistochemistry (IHC) techniques have not been able to interrogate most of these subsets of cells, especially in regard to minority populations or for which there are no defined unique markers, or for the identification of specific functional states within a given subpopulation. But recent improvements in multiplex immunofluorescence (mIF) and spatial analytical technologies have facilitated a better understanding of cellular

heterogeneity, recognizing minor immune cell populations that were difficult to identify and characterize in solid tumors and hematological neoplasms, and allowing inferences regarding cell – cell interactions.¹⁶

Our purpose in this study was to phenotype those minor cell populations using two mIF panels, analyze their spatial distribution, depict their relationship with checkpoint expression (PD-L1, CD137), and identify biomarkers or functional immune states that could be correlated with an unfavorable prognosis.

Materials and methods

Patient samples

We retrospectively retrieved 30 cHL cases (formalin-fixed paraffin-embedded [FFPE] samples from initial lymph node resections) from the Pathology Department of MD Anderson Cancer Center Madrid and UT MD Anderson Cancer Center Houston.

cHL diagnosis was confirmed in all cases by central review and classified according to the 2022 World Health Organization (WHO) classification as: nodular sclerosis cHL (20 cases), mixed cellularity cHL (9 cases), or lymphocyte-rich cHL (1 case). The samples were accompanied by anonymous clinical and laboratory data, treatment, and follow-up information. For initial staging and therapy response criteria, we used the consensus Lugano criteria.¹⁷ Most cases were treated with standard adriamycin-based protocols, such as adriamycin, bleomycin, vinblastine, and dacarbazine (ABVD). Clinical data are summarized in [Table 1](#).

All the samples and data were collected through the MDACC Madrid Biobank, in accordance with the technical and ethical procedures of the Spanish National Biobank Network, including anonymization processes and informed consent, in accordance with the Helsinki Declaration. Approval for this study was obtained from the institutional review board (CEIm H. Ramón y Cajal, reference 445/22).

Chromogenic immunohistochemistry

Initial IHC was performed using an automated staining system (BOND RX; Leica Biosystems, Vista, CA) with antibodies against CD30 to characterize and highlight tumor cells (HRS), immune checkpoint markers (PD-1, PD-L1, CD137), and tumor-infiltrating lymphocyte markers (CD3, PD-1), and markers to characterize monocytic cells and MDSC populations (CD68, CD14, CD33, Arg-1, and CD11b). Cell markers were identified using the Novocastra BOND Polymer Refine Detection Kit (Leica Biosystems, Vista, CA), with a diaminobenzidine reaction to detect antibody labeling and hematoxylin counterstaining. To ensure uniform staining, several tests were performed using different antibody dilutions and antigen retrieval conditions until optimal conditions were obtained for the primary and secondary antibodies in reactive lymph nodes and in tonsil as positive controls. Antibody clones, vendors, and final IHC dilutions are shown in [Table 2](#).

Table 1. Summary of clinical data for cHL patients.

		Total	Unfavorable	Favorable	p
Age	≥65 y	5 (17%)	3 (60%)	2 (40%)	n.s.
	<65 y	24 (83%)	11 (46%)	13 (54%)	
Gender	Male	13 (45%)	7 (54%)	6 (46%)	n.s.
	Female	16 (55%)	7 (44%)	9 (56%)	
cHL subtype	NS	20 (67%)	11 (55%)	9 (45%)	n.s.
	Other (MC or LR)	10 (33%)	3 (30%)	7 (70%)	
Ann Arbor stage	IV	8 (27%)	4 (50%)	4 (50%)	n.s.
	I-III	22 (73%)	10 (45%)	12 (55%)	
IPS	≥3	5 (45%)	2 (40%)	3 (60%)	n.s.
	<3	6 (55%)	2 (33%)	4 (67%)	
Epstein – Barr virus status*	Positive	9 (31%)	4 (44%)	5 (56%)	n.s.
	Negative	20 (69%)	10 (50%)	10 (50%)	
Response to first-line treatment	CR	21 (70%)	5 (24%)	16 (76%)	<0.001
	PR + PD	9 (30%)	9 (100%)	0 (0%)	

NS = nodular sclerosis; MC = mixed cellularity; LR = lymphocyte rich; IPS = international prognostic Score; * EBV in situ hybridization. CR = complete remission; PD = progressive disease; PR = partial response; favorable = PFS >2 y; unfavorable = PFS <2 y; n.s. = non-significant.

Table 2. Details of antibodies used.

Antibody	Clone	Vendor	Dilution for IHC	Dilution for mIF
CD30	Ber-H2	Thermo Fisher Scientific	1:50	1:25
PD-L1	E1L3N	Cell Signaling Technology	1:100	1:1500
CD137	BBK2	Thermo Fisher Scientific	1:50	1:25
CD3	F7.2.38	DAKO	1:100	1:200
PD-1	EPR4877(2) (R)	Abcam	1:250	1:3000
CD68	PG-M1 (M)	DAKO	1:400	1:50
CD11b	EPR1344 (R)	Abcam	1:4000	1:3000
CD14	SP192	Spring	1:200	1:400
CD33	PWS44 (M)	Leica Biosystems	1:100	1:50
Arg-1	D4E3M	Cell Signaling Technology	1:400	1:100

Arg-1 = Arginase-1.

Immunofluorescence

For initial monoplex IF optimization, all antibodies were assessed using the same positive controls as in the IHC optimization, stained using BOND RX autostainer, and linked with fluorophores from the Opal 7 color IHC kit (Akoya Biosciences, Waltham, MA), including 4',6-diamidino-2-phenylindole (DAPI) and Opal tyramide fluorophores (520, 540, 570, 620, 650, and 690). For single IF protocols, after baking and dewaxing (BOND Dewax Solution, Leica Biosystems), the slides were heated at 95°C for 20 min using Bond Antigen Retrieval Tris – ethylenediaminetetraacetic acid buffer or citrate buffer according to the conditions previously determined by IHC to open antibody epitopes. Next, the slides were incubated at room temperature for between 30 and 60 min, depending on the antibody. The slides were washed three times with BOND Wash Solution (Leica Biosystems) and then incubated for 10 min at room temperature with polymer horseradish peroxidase conjugated to anti-mouse/rabbit secondary antibody (Akoya Biosciences). After successive washing, the slides were incubated for 10 min with fluorophores and prepared according to the manufacturer's instructions and counterstained with DAPI for 5 min. The slides were manually mounted with ProLong Diamond Antifade Mountant (Thermo Fisher Scientific, Waltham, MA). For each run of staining, three types of autofluorescence (negative control) slides were carried out in parallel: 1) primary and secondary antibodies; 2) Opal tyramide fluorophores and secondary antibodies; and 3) only secondary antibodies. Negative controls were used to extract endogenous and exogenous autofluorescence from the tissues. Several tests were done

combining antibodies and Opal fluorophores until a specific signal from each antibody was optimized.

Multiplex immunofluorescence and cell phenotype characterization

Once each target was optimized using a monoplex IF protocol, the procedures were combined to obtain the mIF protocol for the different panels. Staining for the different markers was performed consecutively on parallel tissue sections, using the same steps as those for single IF, and detection of each marker was completed before applying the next antibody. Using automated protocols, we set up the sequence of antibodies in each panel and tested each sequence several times until we obtained the same staining pattern as shown in the single IF. Dynamic ranges of the different antibodies linked with their particular fluorophore were set up to obtain similar ranges of expression, with 50–150 ns of exposure time for each antibody, determined by the Vectra-Polaris 3.0.3 scanner system (Akoya Biosciences). The dynamic range of each antibody was carefully adjusted to avoid a cross-talk reaction between fluorophores, or an umbrella effect in which the expression of one antibody can block the expression of another that is expressed in the same cell compartment. For each run of multiplex staining, three types of autofluorescence (negative control) slides were carried out in parallel.

The panels showed a marked ability to identify individual markers and co-localization of several biomarkers in the same cell, thereby characterizing specific predefined cell phenotypes, according to the co-expression of markers shown in Table 3. Granulocytes (neutrophils and eosinophils) cannot be distinguished by their phenotype.

Table 3. Cell phenotypes defined by staining colocalization.

General cell type	Phenotype	Annotation
HRS cells	CD30+/CD3-/CD68- PD-L1-/CD137- PD-L1+	Total HRS cells PD-L1-/CD137- HRS cells Inhibitory HRS cells Co-inhibitory HRS cells
T cells	PD-L1+/CD137+ CD3+/CD30-/CD68- CD137-/PD-1-/PD-L1- PD-1+ CD137+ PDL-1+ PD-1+/PD-L1+	Total T cells Resting T cells Tfh, Antigen-experienced T cells ¹⁸ Activated T cells Exhausted T cells 1 Exhausted T cells 2 ¹⁹
Myeloid cells MDSCs	CD11B+/CD33+/CD30- CD68-/CD14- CD68+/CD14+	Total MDSCs ^{6,20} g-MDSCs m-MDSCs
Monocytic cells	CD68+/CD33-/CD30- PDL1+ CD137+ CD137-/PD1-/PDL1- CD11B+/CD14+/Arg1- CD11B+/CD14+/Arg1+	Total monocytic cells Immunosuppressive monocytic cells Activated monocytic cells Other monocytic cells TAM, M1-like macrophages ²¹ TAM, M2-like macrophages ²¹
Other granulocytic cells*	CD11B+/CD68-/CD14-/CD33-/Arg1-/CD30-	

Tfh = T follicular helper cells. *Other granulocytic cells mainly refer to neutrophils and eosinophils, which cannot be differentiated by their phenotype.

CD137 RNA and protein expression in cell lines

To confirm CD137 RNA expression in neoplastic HRS cells, we used our previously published data obtained from whole-transcriptome expression assays from L-428, L-1236, and KM-H2 cHL-derived cell lines.²² The gene expression data are deposited in Gene Expression Omnibus database under accession number GSE185818.

To analyze protein expression in cell lines using IHC, we used paraffin-embedded cell line pellets prepared with approximately 10^8 cells, washed with PBS, centrifuged, and fixed with buffered formalin (4%). We used exponentially growing KMH2, L-428, L-1236, and HeLa (epithelial cells as negative control), cultured in RPMI-1640 medium. All cell lines were obtained from the German Collection of Microorganisms and Cell Cultures (DSMZ, Braunschweig, Germany).

Independent analyses of CD137 and PD-L1 expression in primary tumors

Additional evaluation of CD137 and PD-L1 IHC protein expression in primary tumors was done using tissue microarrays (TMAs) containing an independent cohort of 130 cHL lymph node samples, obtained from the MDACC Madrid Biobank repositories. TMA sections were stained using the IHC conditions and protocol described above. The number of CD137+ HRS cells and CD137+ immune cells were directly evaluated by one of the authors (JLS). The expression was semi-quantitatively scored by “H-score” (the percentage of positive cells (0–100%) multiplied by the dominant staining intensity score [0/1/2/3+]). For PD-L1 IHC analyses, due to its extensive expression in tumor cells and immune components of the TMA, we applied automated digital analyses of scanned TMA slides generated with Aperio CS2 image capture device (Leica Biosystems) and the IHC Membrane Image Analysis algorithm in Aperio ImageScope software.

Data analysis

For data analyses, mIF stained tissue sections were scanned using the Vectra Polaris multispectral imaging system (Akoya Biosciences). After a whole-slide scan, we selected five matched regions of interest (ROIs) at 20× magnification per patient, identified as the most representative areas and enriched in CD30+ HRS cells by IHC. We used InForm Software 2.3 (Akoya Biosciences) to phenotype the different cell subsets found in both panels. After setting up a different algorithm in each case to recognize the cell morphology, we trained it to identify the cell subsets that had at least 100 cells. To diminish the effect of heterogeneity within each patient’s sample, quantitative data were condensed to the averages of the 5 ROIs for each case. Finally, we exported the data containing the phenotype and the spatial coordinates of each cell in micrometers, and the density and percentage of the different cell populations.

For each panel, and in every cell type and case, the ratio of the cell amount divided by the total quantity of measured cells per patient was calculated. Distances were obtained from the Cartesian coordinates of each cell provided by the InForm application following pipelines developed in R (R 4.2.1 - R Foundation for Statistical Computing). Briefly, data were extracted, and distances calculated using the spatstat package in R, using the nearest neighbor function between two patterns. As there were several ROIs per patient, average distances were calculated for each patient and every pair of cell types.

Each variable was then analyzed independently by R pipelines, and the significance determined using Student’s t-test (if normal) or the non-parametric Kruskal–Wallis test (otherwise). Statistical significance was concluded for values of $p < 0.05$. Univariate proportional hazards (Cox) regression analysis and division into tertiles and quartiles were employed for survival analysis, using progression-free survival (PFS) as the end point. Patient outcome was considered favorable (F) for PFS greater than 2 y, or unfavorable (U) for PFS up to 2 y.

In addition, each variable was dichotomized into high- and low-expression groups, using 33% as the cut-point, chosen as representative of the percentage of non-responders (up to 10% of advanced-stage patients will not reach complete remission and 20–30% of responders eventually relapse).^{23,24}

Patient survival was estimated by the Kaplan–Meier method. Survival curves were compared using the log-rank test between those groups. Finally, correlations for pairs of cell distance and cell frequency values were calculated using Spearman rank analysis and linear regression. All correlations with clinical variables (response or survival) were analyzed using ratios (proportions).

Results

Identification and mapping of scarce cell phenotypes by mIF

Thirty primary FFPE tumor samples were stained with robust 6-color immunofluorescence panels optimized to identify different HRS, T, and myeloid cell types, based on specific marker combinations. Staining and imaging were designed to highlight cell subsets that lack unique immunohistochemistry markers but may mediate immunosuppression in cHL (Figure 1(a)). Colocalization analysis was able to identify 20 individual cell phenotypes based on coordinated protein expression (Figure 1(b)). Automated multi-spectral imaging and analysis calculated cell densities and spatial relationships across matched intratumoral regions.

The majority of the phenotyped cells (34%) were “resting T cells”, which correspond to the T cells that do not express any of the measured checkpoints (Figure 2(a)). Selected areas were enriched in tumor cells, representing 6% of all the cells measured overall. Within that compartment, the minor phenotypes corresponded to the most immunosuppressive signatures: “inhibitory HRS cells”, which expressed PD-L1 (0.9%), and “co-inhibitory HRS cells”, which also co-expressed CD137 (0.3%). In addition, other immunosuppressive subsets that express CD137 were identified in small quantities, such as “activated T cells” (0.5%), and “activated monocytic cells” (0.1%). Detailed information and the number of different cell types identified in each patient are available in **Supplementary Table S1**. Of note, there were no significant differences in statistical results when ratios were calculated using the total number of phenotyped cells or the total number of nucleated cells as the denominator.

As expected, the initial analyses mapping all the cHL profiles showed remarkable heterogeneity among patients, highlighting the importance of individual immune fingerprints of the TME. The relative abundances of specific HRS cells, T cells, and myeloid phenotypes in each case are shown in Figure 2(b). In this cohort, monocytic cells were one of the major populations in the selected HRS-rich ROIs (average, 22%). However, the total percentage of CD68+ cells was not statistically significantly correlated with any of the clinical variables.

Immune and tumor cells expressing CD137 are linked to poor responses to treatment in cHL

Strikingly, the specific immune cell phenotypes of T lymphocytes and monocytic cells that were enriched in patients

with unfavorable clinical evolution were those that co-expressed CD137 (cell ratios: activated T cells: F patients: 0,0047, U patients: 0,0171; activated monocytic cells: F patients: 0,001, U patients: 0,0026; co-inhibitory HRS cells: F patients: 0,0037; U patients: 0,009). Although these “activated T lymphocytes” and “activated monocytic cells” were minor populations, they were significantly associated with PFS (Cox regression, $p = 0.007$ and 0.008 ; and Kaplan–Meier analysis, $p = 0.019$ and 0.001 , respectively) (See Supplementary Figure S1). Remarkably, the subgroup of “co-inhibitory HRS cells” expressing both PD-L1 and CD137 also had significantly worse survival curves, as revealed by Cox regression ($p = 0.010$) and Kaplan–Meier ($p = 0.072$) analyses (Figure 3(a)).

We confirmed these observations using an independent cohort of cHL patients, in which the total number of CD137-expressing cells was associated with unfavorable clinical responses (Kruskal–Wallis test, $p = 0.024$). Indeed, both immune and tumoral HRS cells that expressed CD137, counted independently, were more frequent in patients with shorter PFS (Kaplan–Meier log-rank test, $p = 0.018$ and 0.017 , respectively) (Figure 3(b)), thereby confirming that the CD137 checkpoint plays a relevant role in the pathogenesis of the disease and the configuration of the TME. The expression of CD137 by the neoplastic HRS cells was also confirmed at the RNA and protein levels using cHL-derived cell lines (Figure 3(c)).

A relationship between the expression of CD137 and the presence of Epstein – Barr Virus (EBV) has previously been reported; some studies have found that the viral oncoprotein LPM1 can activate the P13K-AKT-mTOR and pS6K signaling, resulting in increased CD137 surface expression in HRS cells.^{25,26} In our cohort, we did not find any significant correlation between EBV status or disease stage and the expression of CD137 in immune or HRS cells.

Cells expressing CD137 are close to each other in refractory patients

Multiplex immunofluorescence cell maps enable calculation of intercellular proximities using computational pipelines. The pairwise distance between each cell of interest was derived from their Cartesian coordinates. By averaging over all cell pairs, mean proximity relationships between phenotypes were determined for each patient ROI. The CD137 content was also visually higher in refractory patients (representative cases shown in Figure 4(a)).

Cell distances between cell types with significant differences for favorable and unfavorable patients are represented in Figure 4(b), which shows that activated T lymphocytes were closer to the co-inhibitory HRS cells in patients with unfavorable clinical evolution (Cox regression, $p = 0.005$; Kaplan–Meier analysis, $p = 0.004$), consistent with the fact that HRS cells might protect themselves by co-expressing PD-L1 and CD137 on their surface, attracting activated but ineffective populations of T lymphocytes and monocytic cells. In fact, activated T cells and monocytic cells were both closer in refractory cases (Kruskal–Wallis test, $p = 0.012$; Kaplan–Meier analysis, $p = 0.004$). In addition, the “exhausted T cells” (PD-1+/PD-L1+) were slightly more abundant in refractory patients

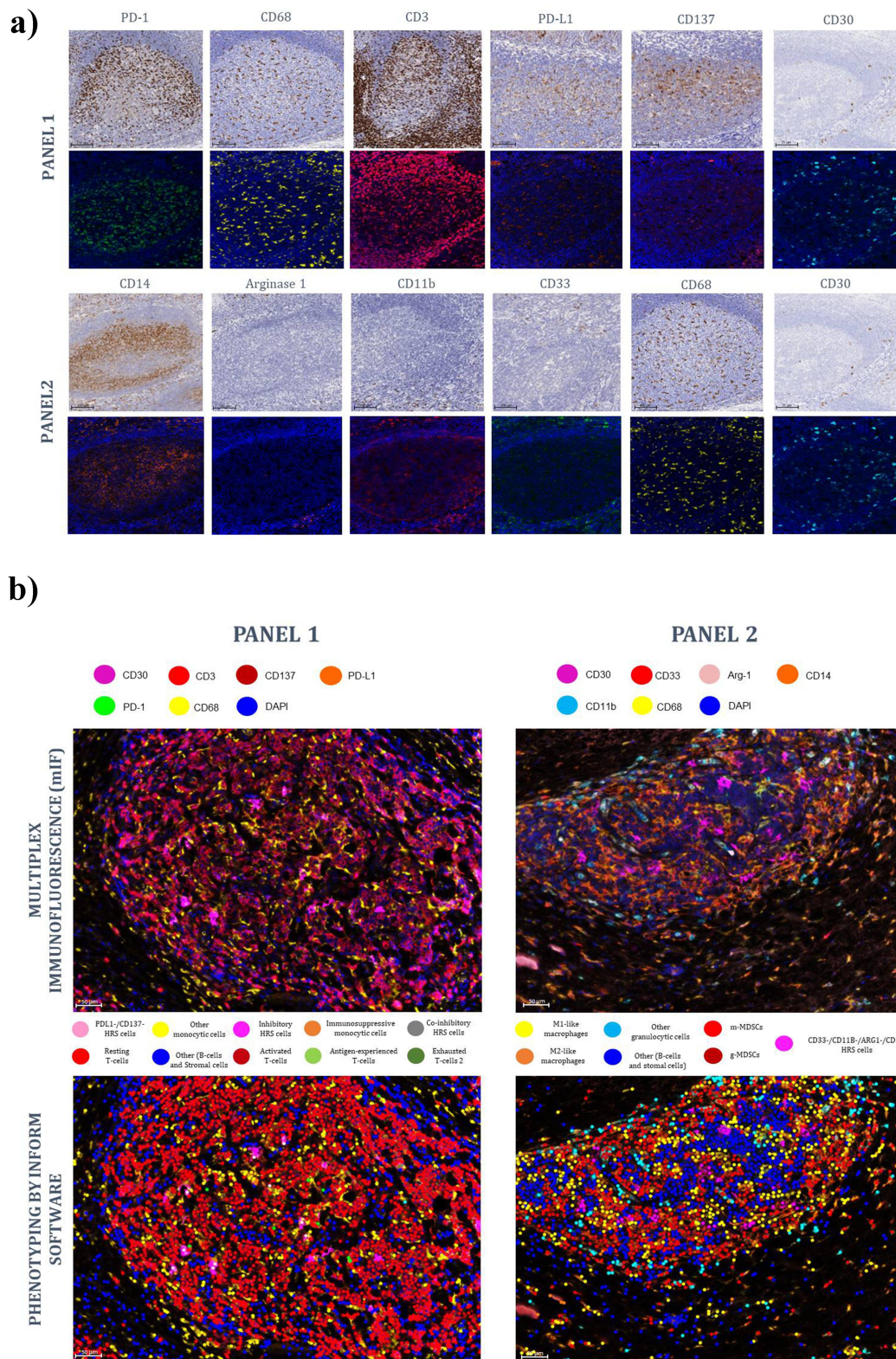
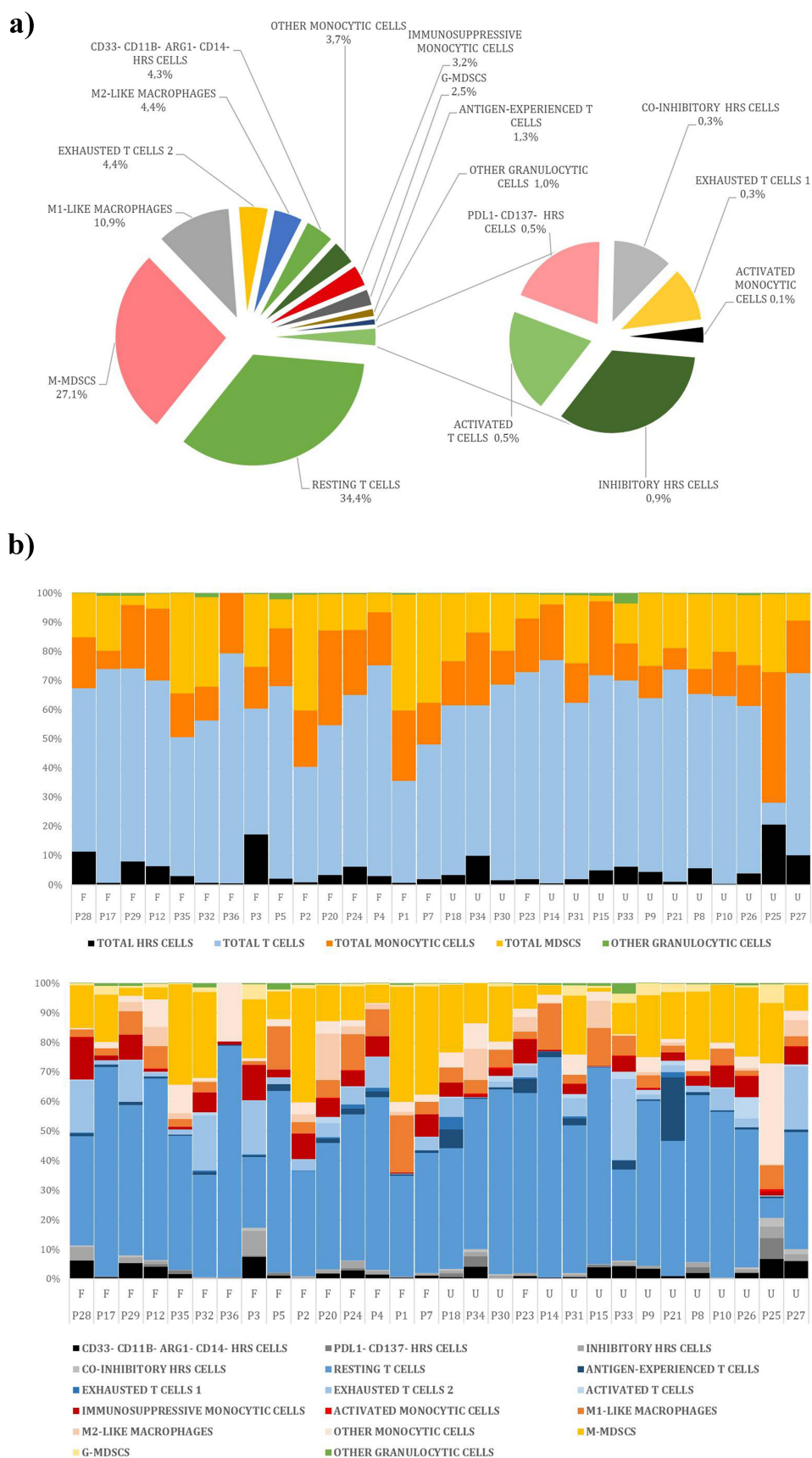


Figure 1. Multiplex immunofluorescence panel design and colocalizations, representative images. (a) The first panel design included PD-1, PD-L1, CD68, CD30, CD137, and CD3 markers. The second panel also included CD30 and CD68, with Arginase-1, CD11B, CD33, and CD14. (b) Inform software colocalizes multiple markers to identify specific cell phenotypes.

(Cox regression, $p = 0.083$) and situated closer to the activated T lymphocytes (Student's t-test, $p = 0.004$; Cox regression, $p = 0.029$). This may be a consequence of the cells closest to HRS adopting an exhausted phenotype.

MDSC subtypes affect prognosis through their amounts and distributions

As noted before in diffuse large B-cell lymphomas (DLBCLs),²⁷ m-MDSCs (CD11B+/CD33+/CD30-/CD68+/CD14+)



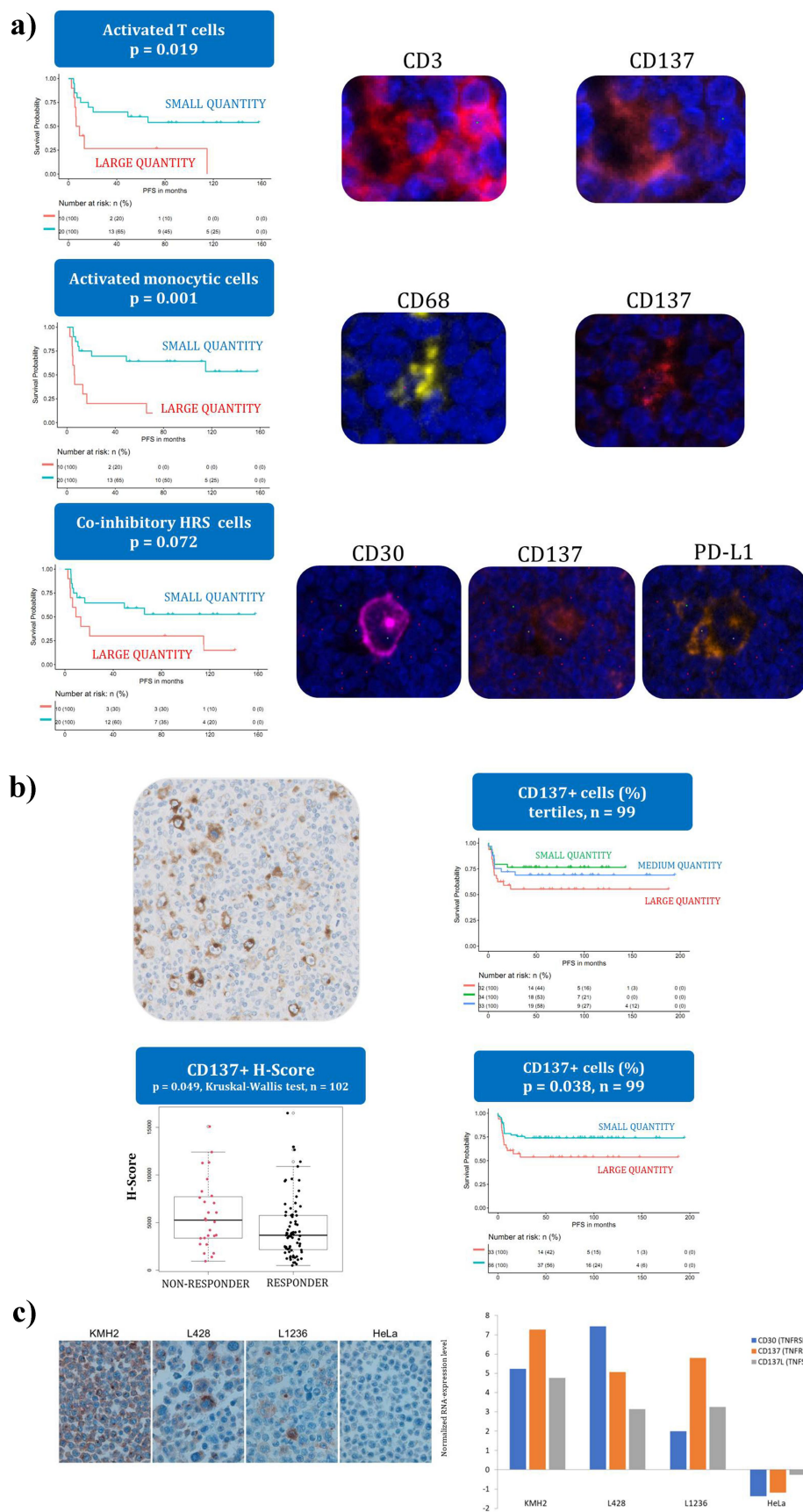


Figure 3. CD137 as a relevant potential biomarker in cHL. (a) Kaplan–Meier plots for immune and tumor cells expressing CD137 and conferring a bad outcome. (b) Representative image of IHC with CD137-stained immune and tumor cells. Boxplot and Kaplan–Meier plots show the increase in the general number of CD137+ cells in refractory patients, with the same effect in tumor and immune cells. (c) CD137 protein expression in cHL-derived cell lines (left) using IHC, and CD137 mRNA expression levels compared with CD30 and CD137L as control genes (right). For the Kaplan–Meier analyses depicted in A and B, small quantity and large quantity dichotomization as described in data analyses.

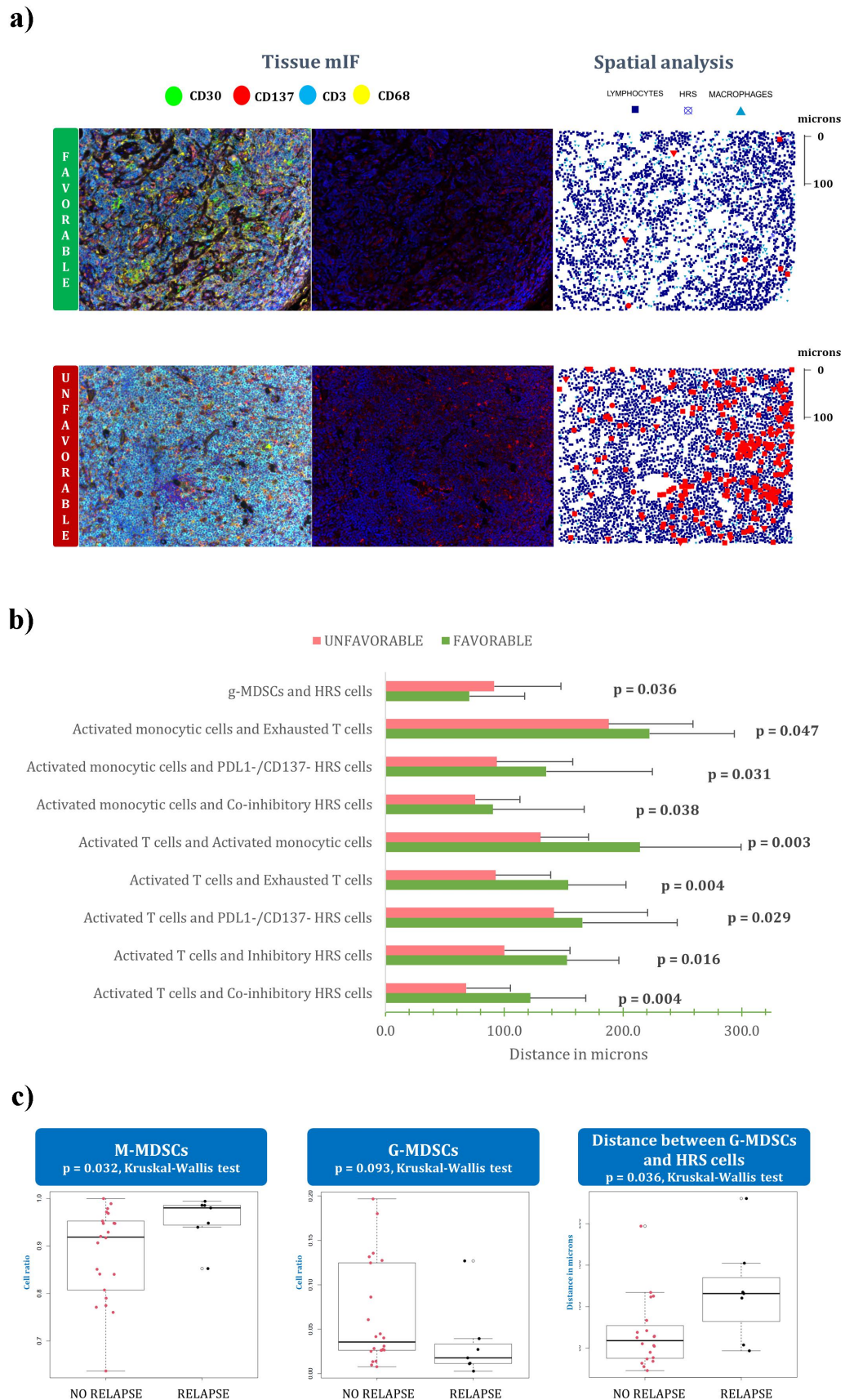


Figure 4. Spatial analysis and MDSC influence in cHL. (a) Representative ROIs of one favorable patient and one non-responder. On the left, the real multiplex immunofluorescence image. Center: IF image with CD137. On the right, the computational analysis is illustrated. The CD137 content, in red, is much higher in the refractory patient. (b) Cellular distances between pairs of cells in micrometers for favorable and unfavorable clinical outcomes, significant results. (c) Boxplots for m-MDSCs and g-MDSCs amounts, and for the distance between HRS cells and g-MDSCs.

of the major populations (27%), unlike what occurred in g-MDSCs (CD11B+/CD33+/CD30-/CD68-/CD14-), which represented only 2.5% of the measured cells. It is of particular note that m-MDSCs became more abundant in patients who relapsed (Kruskal–Wallis test, $p = 0.032$). In contrast, the frequency of g-MDSCs was higher in patients who did not relapse, although the difference was not significant (Kruskal–Wallis test, $p = 0.093$). These associations were consistent with the spatial analysis, as the distance between g-MDSCs and HRS cells was shorter among the patients that did not relapse (Kruskal–Wallis test, $p = 0.036$) (Figure 4c). It suggests that MDSC subtypes have opposing roles in the evolution of the disease, showing more immunosuppressiveness from m-MDSCs than from g-MDSCs. Since MDSCs represent minor populations and were phenotyped in a different panel, we couldn't analyze relationships with CD137-positive cells.

Cell polarization and immune checkpoint expression are globally coordinated by the cHL TME

In the mIF cohort, the number of HRS PD-L1+ cells was not significantly associated with survival (Kaplan–Meier and Cox analysis), probably due to the low number of cases. However, we confirmed that PD-L1 expression was linked to inferior survival in our validation cohort (Kaplan–Meier analysis, $p = 0.042$), as expected.²⁸ Surprisingly, in the same cHL cases, we found a positive correlation between their PD-L1 level and CD137 cell number (Kruskal–Wallis test, $p < 0.001$, $n = 101$) (Figure 5a). This suggests that the TME immune orchestration involves the increase of both immune checkpoints simultaneously. Thus, the unfavorable environment, which may be correlated with early relapses or poor treatment responses, could be shaped by several immune-escape mechanisms acting together.

Going further, linear regression analysis showed that when cell populations expressing PD-L1 increase, those cell populations that do not express become smaller. This happens to all the studied phenotypes: HRS cells, T lymphocytes, and monocytic cells (adjusted R-squared values of 0.88, 0.78, and 0.81, respectively). For HRS and T cells, CD137 shows the same behavior, as seen by their negative Spearman correlation coefficients (-0.62 and -0.67) (Figure 5(b)). These inverse correlations could mean that cells polarize from negative to positive phenotypes for PD-L1 and CD137, or that cell dynamics change to attract CD137-expressing cells or PD-L1-expressing populations to the tumor-rich area, instead of there being merely an increase in their total numbers.

For both CD137 and PD-L1, we observed positive Spearman correlation coefficients among HRS, T, and monocytic cells, indicating that CD137-expressing phenotypes and PD-L1-positive cells are recruited or augmented together (Figure 5(c)). Also, all distances between CD137-expressing phenotypes become shorter at the same time (Figure 5(d)). This could be a consequence of recruitment processes or cell polarization, with consequent increased quantities in such tumor-rich areas.

Discussion

As a key element of the evolutionary process in tumor growth and progression, the TME has been attracting increasing

attention in research and drug development. Therapies targeting TME should be specifically directed to cancer-related phenotypic changes in the non-tumor cells to avoid potential adverse effects. To achieve this requires an in-depth understanding of the differences between the pro-tumor host cells in the TME and the normal host cells at the molecular and cellular levels. To complicate matters, recent studies have found that the immune cells in the TME show significantly increased heterogeneity of cell states and marked phenotypic expansions compared with those in blood and normal tissues.²⁹

One major barrier to deciphering and targeting lymphoma TME is its complexity. The TME of cHL, as in many other tumors, comprises numerous cell types, each of which consists of heterogeneous subsets with various phenotypes and diverse functions. On the other hand, the phenotype and function of cells in the TME may be highly dependent on their exact spatial location and interaction with adjacent immune cells and cancer cells. Here, we confirm how coupling cell phenotyping using mIF with spatial information offers in-depth mechanistic insights into cell–cell interactions and relationships among different cellular components. In addition, the correlation of this information with relevant clinical data allows the description of specific cell niches surrounding HRS cells that are specifically enriched in non-responder patients. This area immediately surrounding the tumor cells is distinctively enriched in m-MDSCs and T cells with an exhausted phenotype, and tumor and immune cells display striking overexpression of PD-L1 and CD137.

The immune system of cancer patients might be impaired by the presence of immunosuppressive cells present in the TME, including MDSCs, regulatory T cells (Tregs), and others, and this may counteract the efficacy of new treatment modalities.³⁰ MDSCs are thought to be immature, and two types have been reported, m-MDSCs and g-MDSCs,⁹ both characterized by cytotoxic CD8+ T cell-suppressive activities.²⁵ M-MDSCs might be derived from the monocyte lineage, but unfortunately, single markers used so far do not differentiate them from true monocytes, or, in many cases, from immature neutrophils. Thus, few studies have identified this myeloid compartment with comprehensive and functional resolution.³¹ Our findings show that the immunosuppressive milieu in refractory patients is enriched by m-MDSC, complementing the results of other studies.⁹ Remarkably, we also found that the abundance of g-MDSC was related to better outcomes and no relapse, a hitherto unreported observation that contrasts with those of other studies in which the quantity of g-MDSC in peripheral blood was correlated with unfavorable prognostic index scores and a shorter PFS.¹⁶ It seems likely that g-MDSCs from the bone marrow and blood can change their functional state in the tumor tissue, depending on its spatial proximity to the HRS cells or other immune components.

Our findings confirm that CD137 is a potential biomarker in the cHL TME, not only as a differential phenotype for the HRS cells,^{13,32} but also as a target for antibody drug conjugates,³³ which may represent an alternative therapeutic option. CD137 is expressed by several types of immune cells, endothelial cells, and some tumor cells.^{34,35} Under normal conditions, activated T lymphocytes that co-express CD137 crosslink with the CD137 ligand (CD137L),

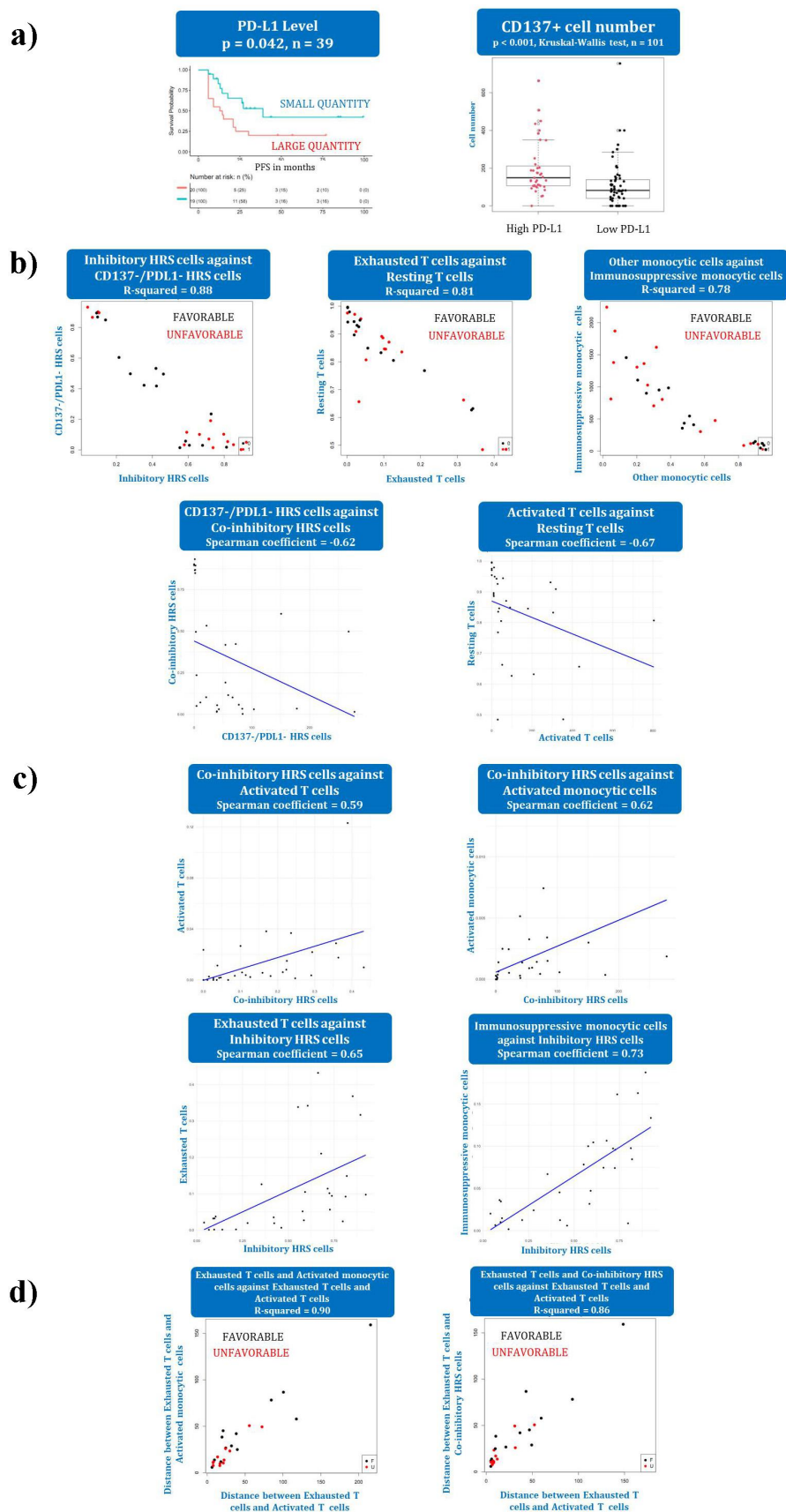


Figure 5. CD137 and PD-L1 are related and coordinate the cHL TME. (a) Kaplan–Meier plot of PD-L1 level dichotomized into high and low groups by the median. The same dichotomization is shown in the boxplot in relation to CD137 cell number. (b) HRS cells, T lymphocytes, and monocytic cells expressing PD-L1 are inversely correlated with their PD-L1- counterparts, as revealed by regression analysis. Spearman coefficients also identify this relationship for CD137 in HRS and T cells. (c) On top, Spearman coefficients for CD137-expressing cell types against each other. Below, the same for PD-L1. (d) Distances of CD137-expressing cells against exhausted T cells showing positive association based on Spearman coefficients.

expressed in antigen-presenting cells to form a complex that polarizes T cells toward a Th1 phenotype and triggers type 1 cytotoxic T cell responses.^{36,37} Our results showing an association between CD137 and poor prognosis could be somehow counterintuitive, since CD137 is generally considered to be expressed in activated T-cells and provides positive co-stimulatory signals. Though, the interpretation that CD137+ expressing cells in the TME have some immunosuppressive character in cHL is also in line with recent data from our group using spatial transcriptomics and cell deconvolution, which confirmed CD137-associated pathways related with adverse outcomes.³⁸ Since with the panels designed in this work, we cannot evaluate the co-expression of CD137 vs CD4/CD8 or NK-markers, additional research and more specific panels will also be necessary.

HRS cells are known to be able to acquire the expression of CD137 by trogocytosis, which is commonly observed among immune cells during close cell – cell contacts, as an additional mechanism for immune escape.³⁹ However, most of the available functional studies of CD137 in HRS cells are based on cHL-derived cell lines, rather than on primary HRS cells. As far as we are aware, this is the first study to show the correlation between CD137+ HRS cells and CD137+ immune cells in primary tumors. In addition, our results confirm that CD137 is actively produced by neoplastic HRS cells in cell lines and primary tumors.

The findings are consistent with those of previous studies, which reported CD137 expression by the HRS cells in 57% to 86% of cHL cases.^{25,40} This not only transduces an activation signal into HRS cells but also dampens immune activation. In murine models, when B and T cells interact, a trogocytic transfer of CD137 from T to B cells and a downregulation of CD137L in B cells were observed.⁴¹ Similarly, CD137 expressed in HRS cells can bind CD137L and cause the internalization of CD137L in the HRS cells themselves as well as in surrounding antigen-presenting cells, resulting in reductions in effective immune cell proliferation and IFN- γ secretion.¹⁵ We hypothesized that not only do the HRS protect themselves by expressing PD-L1 but also CD137 in its surface.

The dependence of cancer cells on the TME has been shown to offer an opportunity for therapeutic intervention by targeting TME elements or its related signaling pathways. Here, we also illustrate the relevance of the spatial distribution of these immune cell populations in relation to the clinical course of patients, and confirm their plasticity and dependence on recruitment by the HRS cells. Finally, we also confirm the potential usefulness of CD137 as a therapeutic target.

Disclosure statement

No potential conflict of interest was reported by the author(s).

Funding

This work was supported by Instituto de Salud Carlos III (ISCIII), projects PI19/00083 and PI22/00556 (co-funded by the European Union), and a Roche Foundation Research Grant. V.M. is a recipient of a Predoctoral Grant from ISCIII FIS (PFIS ref. FI20/00184) and the MD Anderson Foundation scholarship for projects in translational oncology 2022.

ORCID

Juan F. García  <http://orcid.org/0000-0001-6974-0806>

Authorship contributions

J.L.S and V.M. designed the study, performed the research, analyzed the results, created the figures, and wrote the paper; E.P., L.S., R.S., S.F., E.D., A.F.-C., M.J., and A.T. performed the research and analyzed the results; J. K. and C.M. provided samples and clinical data, and analyzed the results; M.G.-C. and F.C. provided samples and clinical data for the validation series, analyzed the results, and reviewed the statistical analysis and the final manuscript. C.D.A. and I.M. provided reagents and analyzed the results; I.W. designed the research and provided equipment and protocols; J.F.G. designed the research, provided funds, analyzed the results, and wrote the paper.

References

- Opinto G, Agostinelli C, Ciavarella S, Guarini A, Maiorano E, Ingravallo G. Hodgkin Lymphoma: a special microenvironment. *J Clin Med*. 2021;10(20):4665. doi:10.3390/jcm10204665.
- Menéndez V, Solórzano JL, Fernández S, Montalbán C, García JF. The Hodgkin lymphoma immune microenvironment: turning bad news into good. *Cancers (Basel)*. 2022;14(5):1360. doi:10.3390/cancers14051360.
- Gunes EG, Rosen ST, Querfeld C. The role of myeloid derived suppressor cells in hematologic malignancies. *Curr Opin Oncol*. 2020;32(5):518–526. doi:10.1097/CCO.0000000000000662.
- Sun R, Zheng Z, Wang L, Cheng S, Shi Q, Qu B, Fu D, Leboeuf C, Zhao Y, Ye J. et al. A novel prognostic model based on four circulating miRNA in diffuse large B cell lymphoma: implications for the roles of MDSC and Th17 cells in lymphoma progression. *Mol Oncol*. 2021;15(1):246–261. doi:10.1002/1878-0261.12834.
- Calabretta E, d'Amore F, Carlo-Stella C. Immune and inflammatory cells of the tumor microenvironment represent novel therapeutic targets in classical Hodgkin Lymphoma. *Int J Mol Sci*. 2019;20(21):5503. doi:10.3390/ijms20215503.
- Elliott LA, Doherty GA, Sheahan K, Ryan EJ. Human tumor-infiltrating myeloid cells: phenotypic and functional diversity. *Front Immunol*. 2017;8:86. doi:10.3389/fimmu.2017.00086.
- McKee SJ, Tuong ZK, Kobayashi T, Doff BL, Soon MS, Nissen M, Lam PY, Keane C, Vari F, Moi D. et al. B cell lymphoma progression promotes the accumulation of circulating Ly6Clo monocytes with immunosuppressive activity. *Oncoimmunology*. 2017;7(2):e1393599. doi:10.1080/2162402X.2017.1393599.
- Vari F, Arpon D, Keane C, Hertzberg MS, Talaulikar D, Jain S, Cui Q, Han E, Tobin J, Bird R. et al. Immune evasion via PD-1/PD-L1 on NK cells and monocyte/macrophages is more prominent in Hodgkin lymphoma than DLBCL. *Blood*. 2018;131(16):1809–1819. doi:10.1182/blood-2017-07-796342.
- Romano A, Parrinello NL, Vetro C, Tibullo D, Giallongo C, La Cava P, Chiarenza A, Motta G, Caruso AL, Villari L. et al. The prognostic value of the myeloid-mediated immunosuppression marker arginase-1 in classic Hodgkin lymphoma. *Oncotarget*. 2016;7(41):67333–67346. doi:10.18632/oncotarget.12024.
- Roemer MGM, Advani RH, Ligon AH, Natkunam Y, Redd RA, Homer H, Connelly CF, Sun HH, Daadi SE, Freeman GJ. et al. PD-L1 and PD-L2 genetic alterations define classical Hodgkin lymphoma and predict outcome. *J Clin Oncol*. 2016;34(23):2690–2697. doi:10.1200/JCO.2016.66.4482.
- Green MR, Monti S, Rodig SJ, Juszczynski P, Currie T, O'Donnell E, Chapuy B, Takeyama K, Neuberg D, Golub TR. et al. Integrative analysis reveals selective 9p24.1 amplification, increased PD-1 ligand expression, and further induction via JAK2 in nodular sclerosing Hodgkin lymphoma and primary mediastinal large B-cell lymphoma. *Blood*. 2010;116(17):3268–3277. doi:10.1182/blood-2010-05-282780.

12. Ansell SM, Lesokhin AM, Borrello I, Halwani A, Scott EC, Gutierrez M. et al. PD-1 blockade with nivolumab in relapsed or refractory Hodgkin's lymphoma. *N Engl J Med.* 2015;372:311–319. doi:10.1056/NEJMoa1411087.
13. Anderson MW, Zhao S, Freud AG, Czerwinski DK, Kohrt H, Alizadeh AA, Houot R, Azambuja D, Biasoli I, Morais JC. et al. CD137 is expressed in follicular dendritic cell tumors and in classical Hodgkin and T-cell lymphomas: diagnostic and therapeutic implications. *Am J Pathol.* 2012;181(3):795–803. doi:10.1016/j.ajpath.2012.05.015.
14. Rajendran S, Ho WT, Schwarz H. CD137 signaling in Hodgkin and Reed-Sternberg cell lines induces IL-13 secretion, immune deviation and enhanced growth. *Oncoimmunology.* 2016;5(6):e1160188. doi:10.1080/2162402X.2016.1160188.
15. Ho WT, Pang WL, Chong SM, Castella A, Al-Salam S, Tan TE, Moh MC, Koh LK, Gan SU, Cheng CK. et al. Expression of CD137 on Hodgkin and Reed-Sternberg cells inhibits T-cell activation by eliminating CD137 ligand expression. *Cancer Res.* 2013;73(2):652–661. doi:10.1158/0008-5472.CAN-12-3849.
16. Aoki T, Steidl C. Novel insights into Hodgkin lymphoma biology by single-cell analysis. *Blood.* 2023;141(15):1791–1801. doi:10.1182/blood.2022017147.
17. Ricard F, Cheson B, Barrington S, Trotman J, Schmid A, Brueggerwerth G, Salles G, Schwartz L, Goldmacher G, Jarecha R. et al. Application of the Lugano classification for initial evaluation, staging, and response assessment of Hodgkin and Non-Hodgkin Lymphoma: the PRoLoG consensus initiative (part 1—clinical). *J Nucl Med.* 2023;64(1):102–108. doi:10.2967/jnumed.122.264106.
18. Sharpe AH, Pauken KE. The diverse functions of the PD1 inhibitory pathway. *Nat Rev Immunol.* 2018;18(3):153–167. doi:10.1038/nri.2017.108.
19. Lee J, Ahn E, Kissick HT, Ahmed R. Reinvigorating exhausted T cells by blockade of the PD-1 pathway. *Forum Immun Dis Ther.* 2015;6(1–2):7–17. doi:10.1615/ForumImmunDisTher.2015014188.
20. Lechner MG, Megiel C, Russell SM, Bingham B, Arger N, Woo T, Epstein AL. Functional characterization of human Cd33+ and Cd11b+ myeloid-derived suppressor cell subsets induced from peripheral blood mononuclear cells co-cultured with a diverse set of human tumor cell lines. *J Transl Med.* 2011;9(1):90. doi:10.1186/1479-5876-9-90.
21. Boutilier AJ, ElSawa SF. Macrophage polarization states in the tumor microenvironment. *Int J Mol Sci.* 2021;22(13):6995. doi:10.3390/ijms22136995.
22. Fernández S, Solórzano JL, Díaz E, Menéndez V, Maestre L, Palacios S, López M, Colmenero A, Estévez M, Montalbán C. et al. JAK/STAT blockade reverses the malignant phenotype of Hodgkin and Reed-Sternberg cells. *Blood Adv.* 2023;7(15):4135–4147. doi:10.1182/bloodadvances.2021006336.
23. Mohty R, Dulery R, Bazarbachi AH, Savani M, Hamed RA, Bazarbachi A, Mohty M. Latest advances in the management of classical Hodgkin lymphoma: the era of novel therapies. *Blood Cancer J.* 2021;11(7):1–10. doi:10.1038/s41408-021-00518-z.
24. Van Den Neste E, Casasnovas O, André M, Touati M, Senecal D, Edeline V, Stamatoullas A, Fornecker L, Deau B, Gastinne T. et al. Classical Hodgkin's lymphoma: the lymphoma study association guidelines for relapsed and refractory adult patients eligible for transplant. *Haematologica.* 2013;98(8):1185–1195. doi:10.3324/haematol.2012.072090.
25. Aravindh SP, Rajendran S, Li Y, Wu M, Yi Wong AH, Schwarz H. Epstein-Barr virus-encoded LMP1 induces ectopic CD137 expression on Hodgkin and Reed-Sternberg cells via the PI3K-AKT-mTOR pathway. *Leuk Lymphoma.* 2019;60(11):2697–2704. doi:10.1080/10428194.2019.1607330.
26. Yoshimori M, Imadome K-I, Komatsu H, Wang L, Saitoh Y, Yamaoka S, Fukuda T, Kurata M, Koyama T, Shimizu N. et al. CD137 expression is induced by Epstein-Barr virus infection through LMP1 in T or NK cells and mediates survival promoting signals. *PLOS ONE.* 2014;9(11):e112564. doi:10.1371/journal.pone.0112564.
27. Wang Z, Jiang R, Li Q, Wang H, Tao Q, Zhai Z. Elevated M-MDSCs in circulation are indicative of poor prognosis in diffuse large B-Cell lymphoma patients. *J Clin Med.* 2021;10(8):1768. doi:10.3390/jcm10081768.
28. Hollander P, Kamper P, Smedby KE, Enblad G, Ludvigsen M, Mortensen J, Amini R-M, Hamilton-Dutoit S, d'Amore F, Molin D. et al. High proportions of PD-1+ and PD-L1+ leukocytes in classical Hodgkin lymphoma microenvironment are associated with inferior outcome. *Blood Adv.* 2017;1(18):1427–1439. doi:10.1182/bloodadvances.2017006346.
29. Gholiha AR, Hollander P, Löf L, Larsson A, Hashemi J, Ulfstedt JM, Molin D, Amini R-M, Freyhult E, Kamali-Moghaddam M. et al. Immune-proteome profiling in classical Hodgkin lymphoma tumor diagnostic tissue. *Cancers (Basel).* 2021;14(1):9. doi:10.3390/cancers14010009.
30. Kumar V, Patel S, Tcyganov E, Gabrilovich DI. The nature of myeloid-derived suppressor cells in the tumor microenvironment. *Trends In Immunol.* 2016;37(3):208–220. doi:10.1016/j.it.2016.01.004.
31. Stewart BJ, Fergie M, Young MD, Jones C, Sachdeva A, Blain A, Bacon CM, Rand V, Ferdinand JR, James KR. et al. Spatial and molecular profiling of the mononuclear phagocyte network in classic Hodgkin lymphoma. *Blood.* 2023;141:2343–2358. doi:10.1182/blood.2022015575.
32. Carbone PN, Zhang Q-Y. Validation of CD137 Immunohistochemical stain on paraffin-embedded tissue as a Marker to facilitate distinction between classic Hodgkin lymphoma, nodular lymphocyte-predominant Hodgkin lymphoma, T-Cell/Histiocyte-rich large B-Cell lymphoma, and anaplastic large cell lymphoma. *Arch Pathol Lab Med.* 2019;143(3):280–281. doi:10.5858/arpa.2018-0345-LE.
33. Rajendran S, Li Y, Ngho E, Wong HY, Cheng MS, Wang C-I, Schwarz H. Development of a bispecific antibody targeting CD30 and CD137 on Hodgkin and Reed-Sternberg cells. *Front Oncol.* 2019;9. doi:10.3389/fonc.2019.00945.
34. Drenkard D, Becke FM, Langstein J, Spruss T, Kunz-Schughart LA, Tan TE, Lim YC, Schwarz H. CD137 is expressed on blood vessel walls at sites of inflammation and enhances monocyte migratory activity. *Faseb J.* 2007;21(2):456–463. doi:10.1096/fj.05-4739com.
35. Broll K, Richter G, Pauly S, Hofstaedter F, Schwarz H. CD137 expression in tumor vessel walls. High correlation with malignant tumors. *Am J Clin Pathol.* 2001;115(4):543–549. doi:10.1309/E343-KMYX-W3Y2-10KY.
36. Melero I, Shuford WW, Newby SA, Aruffo A, Ledbetter JA, Hellström KE, Mittler RS, Chen L. Monoclonal antibodies against the 4-1BB T-cell activation molecule eradicate established tumors. *Nat Med.* 1997;3(6):682–685. doi:10.1038/nm0697-682.
37. Thum E. CD137, implications in immunity and potential for therapy. *Front Biosci (Landmark Ed).* 2009;14(14):4173–4188. doi:10.2741/3521.
38. Menéndez V, Solórzano JL, García-Cosío M, Cereceda L, Díaz E, Estévez M, Roncador G, Vega Z, Montalbán C, Kulasinghe A. et al. Mapping the spatial dynamics of the CD4+ T cell spectrum in classical Hodgkin lymphoma. *Mod Pathol.* 2024;37(9):100551. doi:10.1016/j.modpat.2024.100551.
39. Taylor RP, Lindorfer MA. Fcγ-receptor-mediated trogocytosis impacts mAb-based therapies: historical precedence and recent developments. *Blood.* 2015;125(5):762–766. doi:10.1182/blood-2014-10-569244.
40. Shi YF, Gao ZF, Liu CL, Huang X, Song YQ, Zhang C, Lin DM, Zhou LX, Zhao M, Lai YM. et al. [Expression of CD137 in tumor cells of Hodgkin lymphoma from Northern China and its application in pathological differential diagnosis]. *Zhonghua Xue Ye Xue Za Zhi.* 2016;37(6):484–490. doi:10.3760/cma.j.issn.0253-2727.2016.06.009.
41. Shao Z, Harfuddin Z, Pang WL, Nickles E, Koh LK, Schwarz H. Trogocytic CD137 transfer causes an internalization of CD137 ligand on murine APCs leading to reduced T cell costimulation. *J Leukoc Biol.* 2015;97(5):909–919. doi:10.1189/jlb.3A0213-079RRR.